

NACA RM L54F23



# RESEARCH MEMORANDUM

COMPARISON BETWEEN THEORETICAL AND EXPERIMENTAL RATES  
OF ROLL OF TWO MODELS WITH FLEXIBLE RECTANGULAR  
WINGS AT SUPERSONIC SPEEDS

By John M. Hedgepeth and Robert J. Kell

Langley Aeronautical Laboratory  
Langley Field, Va.

CLASSIFICATION CANCELLED

Authenticity *NACA Res. Lab.* Date *6/12/56*  
*RN 102*  
By *MTA 6/27/56* See \_\_\_\_\_

RECEIVED  
AUG 10 1954  
LANGLEY AERONAUTICAL LABORATORY  
LANGLEY FIELD, VIRGINIA

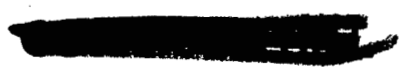
CLASSIFIED DOCUMENT

This material contains information affecting the National Defense of the United States within the meaning of the espionage laws, Title 18, U.S.C., Secs. 793 and 794, the transmission or revelation of which in any manner to an unauthorized person is prohibited by law.

## NATIONAL ADVISORY COMMITTEE FOR AERONAUTICS

WASHINGTON

August 5, 1954



## NATIONAL ADVISORY COMMITTEE FOR AERONAUTICS

## RESEARCH MEMORANDUM

COMPARISON BETWEEN THEORETICAL AND EXPERIMENTAL RATES  
OF ROLL OF TWO MODELS WITH FLEXIBLE RECTANGULAR  
WINGS AT SUPERSONIC SPEEDS

By John M. Hedgepeth and Robert J. Kell

## SUMMARY

A comparison is presented between the experimentally measured and theoretically calculated (by the method of NACA TN 3067) rates of roll of two rocket-propelled models with flexible rectangular wings. The comparisons show that although there are large aeroelastic losses in rolling rate, the theory predicts the actual rate of roll accurately.

## INTRODUCTION

In reference 1, a method is presented for calculating the aeroelastic effects at supersonic speeds on the rolling behavior of aircraft with flexible rectangular wings. The method employs structural influence coefficients to determine the deformations of the wings and linearized supersonic lifting-surface theory to find the airloads.

The purpose of the present paper is to assess the accuracy of the method of reference 1 by comparing its predictions with some experimental data presented in reference 2 for two rocket-powered test models. Comparisons between theory and experiment are given in the form of plots of rolling rate against Mach number.

## SYMBOLS

- D local flexural stiffness,  $Et^3/12(1 - \mu^2)$   
E Young's modulus of elasticity  
G shear modulus of elasticity
- 

GJ	elementary torsional stiffness, $G \int_{-c/2}^{c/2} \frac{t^3(x)}{3} dx$
$\frac{\partial G_m(y,n)}{\partial y}$	structural rate-of-twist influence function which results from a unit concentrated torque
I	moment of inertia of beam that represents flange effect of aileron
K(x)	stiffness of root springs
L(y)	aerodynamic load per unit span, positive upward
M	free-stream Mach number
M(y)	aerodynamic moment, per unit span, about midchord, positive in positive twist direction
P <sub>h</sub>	static pressure at altitude
P <sub>0</sub>	standard static pressure at sea level
Q(y)	aerodynamic moment, per unit span, about elastic axis, positive in positive twist direction
V	free-stream velocity
W(y)	deflection of midchord line of wing, positive upwards
a	ratio between fuselage radius and exposed wing semispan
b	total wing span, $2(al + l)$
c	wing chord
c <sub>a</sub>	aileron chord
e	distance measured forward from midchord to elastic axis, expressed as fraction of chord
l	exposed wing semispan
p	rolling velocity
$\frac{pb}{2V}$	tangent of wing-tip helix angle, positive for counter-clockwise roll when viewed from behind

s	ratio of root flexibility to wing flexibility
t	thickness of wing cross section
w(x,y)	local deflection of wing, positive upwards
x,y	coordinate system
$\bar{x}$	distance from midchord to location of beam that represents flange effect of aileron
$\theta(y)$	angle of twist of wing, leading edge up
$\theta_r$	twist at mid exposed span which results from a unit torque at the tip
$\delta$	aileron deflection, positive down
$\lambda$	nondimensional parameter involved in the rate-of-twist influence function (see eq. (A10))
$\mu$	Poisson's ratio
$\phi$	rolling effectiveness, $\frac{(pb/2V)_F}{(pb/2V)_R}$

## Subscripts:

F	flexible wing
R	rigid wing
rev	aileron reversal

## DESCRIPTION OF THE MODELS

The two models investigated (the last two in table I of ref. 2) were essentially the same in size and shape, the only important difference being that one had aluminum wings and the other had steel. Both models had three rectangular wings equally spaced around the rear portion of a long cylindrical body. (See fig. 1.) The wings were uniform in the spanwise direction and had NACA 65A003 airfoil sections. The full-span trailing-edge ailerons were formed by bending the wing along the 80-percent-chord line.

The pertinent dimensions of the two models are given in table I. Included in table I are the experimentally determined values of  $\theta_r$ , the twist at the midspan due to a unit torque at the tip. These values, which were obtained from reference 2, are used as an aid in determining the structural characteristics of the wings. The ordinates for the NACA 65A003 airfoil, obtained from reference 3, are also included in this table.

### THEORETICAL RESULTS

The experimental data in reference 2 are given in the form of plots of rolling rate  $pb/2V$  against Mach number  $M$ . Also given are the variations with Mach number of altitude (specified in the form of static pressure) during the flights. It is desired to calculate theoretically the variation of  $pb/2V$  with Mach number for the prescribed altitude variation for each of the two models. In order to do this, the computational procedure outlined in reference 1 is followed.

In reference 1, several alternative calculation schemes were described. The particular one used herein is the same as that used in the analysis of the example configuration in reference 1. This approach is exemplified by the matrix equations (29) or (31) of that report. These equations are written in terms of the rate of twist  $d\theta/dy$  rather than the twist  $\theta$  itself and make use of an interpolation procedure to reduce the number of degrees of freedom involved. For the present problem the structural ingredients of these matrix equations - the rate-of-twist influence functions - are derived in the appendix of this report by the application of an approximate plate theory and are tabulated for both models in table II; the aerodynamic ingredients - the various indicial loads and the loads due to roll and aileron deflection - are obtained from reference 1. (The assumption is made that the loads on each wing of the three-winged aircraft considered in this paper are the same as those resulting from the two-winged configuration considered in ref. 1.) It should be noted that the analysis in the appendix indicates the existence of an "elastic axis," a line along which loads can be placed without producing any appreciable twist. Accordingly, equations (29) and (31) of reference 1 are modified as suggested therein to take advantage of this elastic axis.

By using these modified equations, then, and by following the suggested computational procedure, the theoretical results presented herein were obtained. The results for aileron reversal appear in terms of  $(P_h/P_o)_{rev}$ , the ratio between the static pressure at which the ailerons reverse and the standard sea-level static pressure. In figure 2 is shown the variation with Mach number of this ratio for both the aluminum and

steel wings. A calculation of the rolling effectiveness  $\phi = \left(\frac{pb}{2V}\right)_F / \left(\frac{pb}{2V}\right)_R$  for other values of static pressure at several different Mach numbers showed that the variation of  $\phi$  with  $P_h/P_o$  was almost exactly linear. Therefore, the values of  $\phi$  for any pressure ratio at a given Mach number can be deduced from the value of  $\left(P_h/P_o\right)_{rev}$  for that Mach number. Thus, for either model

$$\phi = 1 - \frac{\left(P_h/P_o\right)}{\left(P_h/P_o\right)_{rev}} \quad (1)$$

The rolling rate  $pb/2V$  for the flexible wing can be obtained by multiplying  $\phi$  by  $\left(pb/2V\right)_R$ . Consequently,

$$\left(\frac{pb}{2V/\delta}\right)_F = \left(\frac{pb}{2V/\delta}\right)_R \left[ 1 - \frac{\left(P_h/P_o\right)}{\left(P_h/P_o\right)_{rev}} \right] \quad (2)$$

The variation of  $\left(\frac{pb}{2V/\delta}\right)_R$  with Mach number has been found by the method of reference 1; these values were used in conjunction with the information in figure 2 and the plots of the actual flight values of  $P_h/P_o$  against Mach number from reference 2 to obtain the theoretical values of  $\frac{pb}{2V/\delta}$  shown in figure 3 for the two models. Also shown in figure 3 is the theoretical  $\frac{pb}{2V/\delta}$  for the rigid wing. It should be remarked that measured values of  $P_h/P_o$  were lacking for Mach numbers higher than 1.4 for the steel wing and 1.8 for the aluminum wing; accordingly, the curves for the flexible wings have been stopped at these values.

#### COMPARISONS AND DISCUSSION

The variation of experimental  $\frac{pb}{2V/\delta}$  with Mach number, as obtained from reference 2, is shown in figure 3 for comparison. The estimated experimental rigid rate of roll, obtained by extrapolation from the flexible data by assuming a linear variation of  $pb/2V$  with the parameter  $P_{h\theta_r}$ , is also shown in this figure.

From figure 3 it can be seen that although there is a large loss of rolling effectiveness due to aeroelasticity, the theory does a good job of predicting the actual flexible rate of roll.

#### CONCLUSION

A comparison between theoretically and experimentally determined rates of roll for two rocket-propelled models with flexible rectangular wings shows that the method of NACA TN 3067 is capable of yielding accurate predictions for the aeroelastic effects on the roll of supersonic aircraft with rectangular wings.

Langley Aeronautical Laboratory,  
National Advisory Committee for Aeronautics,  
Langley Field, Va., June 11, 1954.

## APPENDIX

## DERIVATION OF TORSIONAL INFLUENCE COEFFICIENTS

In order to solve the aeroelastic rolling problem it is necessary to compute the torsional influence coefficients for the wing. These quantities are derived in this appendix by means of the same approach as that of reference 4; that is, the deflections are assumed to be linear in the chordwise direction and the principle of minimum potential energy is employed.

The structure under consideration is shown in figure 4(a). It consists of a solid plate that is uniform in the spanwise direction with a bent-up aileron and a more-or-less-rigid attachment to the model body. Two factors prevent the analysis of this structure directly by the method of reference 4: (1) The bend along the aileron hinge line produces a flange effect so that flat-plate theory cannot be used; (2) the root of the wing cannot be considered to be perfectly clamped. The analysis is therefore performed for the equivalent structure shown in figure 4(b). In this figure, the aileron has been unbent and the flange effect has been represented by a beam. The moment of inertia of the beam is assumed to be equal to the difference between the moments of inertia of the bent and unbent aileron and the beam is located at the centroid of the difference-in-moment-of-inertia distribution. Thus,

$$I = \tan^2 \delta \int_{\frac{c}{2} - c_a}^{c/2} t(x) \left( x - \frac{c}{2} + c_a \right)^2 dx \quad (A1)$$

$$\bar{x} = \frac{\int_{\frac{c}{2} - c_a}^{c/2} t(x) \left( x - \frac{c}{2} + c_a \right)^2 x dx}{\int_{\frac{c}{2} - c_a}^{c/2} t(x) \left( x - \frac{c}{2} + c_a \right)^2 dx} \quad (A2)$$

Also, in order to represent the effect of incomplete root clamping, the plate-beam combination is assumed to be mounted on springs which prevent displacement of the root but permit non-zero slopes in the spanwise direction. In the analysis to follow, the shape of the stiffness

distribution of these springs, which, for the present, is indeterminate, is assumed to be such that the resulting equations exhibit their simplest possible form; the absolute magnitude of the spring stiffness for each of the two models is then selected so that the theoretical twist at the midspan due to a unit torque at the tip matches the experimental value in table I.

The potential energy of this equivalent structure subjected to the distributed lateral load  $p(x,y)$  is

$$\begin{aligned} \pi = \frac{1}{2} \int_0^l \int_{-c/2}^{c/2} & \left\{ D(x) \left[ \left( \frac{\partial^2 w}{\partial y^2} \right)^2 + \left( \frac{\partial^2 w}{\partial x^2} \right)^2 + 2\mu \frac{\partial^2 w}{\partial x^2} \frac{\partial^2 w}{\partial y^2} + \right. \right. \\ & \left. \left. 2(1 - \mu) \left( \frac{\partial^2 w}{\partial x \partial y} \right)^2 \right\} dx dy + \frac{EI}{2} \int_0^l \left[ \frac{\partial^2 w(\bar{x}, y)}{\partial y^2} \right]^2 dy + \\ & \frac{1}{2} \int_{-c/2}^{c/2} \left\{ K(x) \left[ \frac{\partial w}{\partial y}(x, 0) \right]^2 \right\} dx - \int_0^l \int_{-c/2}^{c/2} p(x, y) w(x, y) dx dy \end{aligned} \quad (A3)$$

where  $w(x,y)$  is the deflection,  $D(x) = \frac{Et^3}{12(1 - \mu^2)}$  is the plate stiffness, and  $K(x)$  is the stiffness distribution of the root springs.

In accordance with the assumption of linear chordwise deformations, let

$$w(x,y) = W(y) - x\theta(y) \quad (A4)$$

Then, upon performing the integration with respect to  $x$ ,

$$\begin{aligned}
\pi = & \frac{1}{2} \int_0^l \left[ (a_1 + EI) (w'')^2 - 2(a_2 + EIX) w'' \theta'' + \right. \\
& \left. (a_3 + EIX^2) (\theta'')^2 + 2(1 - \mu) a_1 (\theta')^2 \right] dy + \\
& \frac{1}{2} \left[ k_1 (w')^2 - 2k_2 w' \theta' + k_3 (\theta')^2 \right]_{y=0} - \\
& \int_0^l [L(y)W(y) + M(y)\theta(y)] dy \tag{A5}
\end{aligned}$$

where

$$a_n = \int_{-c/2}^{c/2} x^{n-1} D(x) dx$$

$$k_n = \int_{-c/2}^{c/2} x^{n-1} K(x) dx$$

and

$$L(y) = \int_{-c/2}^{c/2} p(x,y) dx$$

$$M(y) = - \int_{-c/2}^{c/2} xp(x,y) dx$$

are, respectively, the section lift and moment about the midchord.

Minimization of the potential energy yields the following differential equations,

$$\left. \begin{aligned} (a_1 + EI)W^{IV} - (a_2 + EI\bar{X})\theta^{IV} &= L \\ - (a_2 + EI\bar{X})W^{IV} + (a_3 + EI\bar{X}^2)\theta^{IV} - 2(1 - \mu)a_1\theta'' &= M \end{aligned} \right\} \quad (A6)$$

and boundary conditions,

$$W(0) = \theta(0) = 0$$

$$(a_1 + EI)W''(0) - (a_2 + EI\bar{X})\theta''(0) - k_1W'(0) + k_2\theta'(0) = 0$$

$$(a_2 + EI\bar{X})W''(0) - (a_3 + EI\bar{X}^2)\theta''(0) - k_2W'(0) + k_3\theta'(0) = 0$$

$$(a_1 + EI)W''(l) - (a_2 + EI\bar{X})\theta''(l) = 0$$

$$(a_2 + EI\bar{X})W''(l) - (a_3 + EI\bar{X}^2)\theta''(l) = 0$$

$$(a_1 + EI)W'''(l) - (a_2 + EI\bar{X})\theta'''(l) = 0$$

$$(a_2 + EI\bar{X})W'''(l) - (a_3 + EI\bar{X}^2)\theta'''(l) + 2(1 - \mu)a_1\theta'(l) = 0$$

For purposes of aeroelastic calculations, only the twist  $\theta$  is important; therefore, it is desirable to eliminate  $W$  from equations (A6) and the accompanying boundary conditions. In order to do this easily, it is convenient to take advantage of the freedom of choice of the shape of the root spring stiffness distribution and assume that

$$\frac{k_1}{a_1 + EI} = \frac{k_2}{a_2 + EI\bar{X}} = \frac{k_3}{a_3 + EI\bar{X}^2}$$

Since, as has been mentioned, the overall spring stiffness is to be selected by duplicating experimental values of twist, this limitation on the distribution should have negligible influence on the desired aeroelastic results.

After eliminating  $W$ , the resulting equations are

$$\left[ a_3 + EI\bar{x}^2 - \frac{(a_2 + EI\bar{x})^2}{a_1 + EI} \right] \theta^{IV} - 2(1 - \mu)a_1\theta'' = M + \frac{a_2 + EI\bar{x}}{a_1 + EI} L \quad (A7)$$

$$\theta(0) = 0$$

$$\theta''(0) = \frac{k_1}{a_1 + EI} \theta'(0)$$

$$\theta''(l) = 0$$

$$\left[ a_3 + EI\bar{x}^2 - \frac{(a_2 + EI\bar{x})^2}{a_1 + EI} \right] \theta''''(l) - 2(1 - \mu)a_1\theta'(l) = 0$$

Integrating equation (A7) once and rewriting yields

$$\theta'''' - \frac{\lambda^2}{l^2} \theta' = -\frac{\lambda^2}{l^2} \frac{1}{GJ} \int_y^l Q(\eta) d\eta \quad (A8)$$

where the remaining boundary conditions are

$$\left. \begin{aligned} \theta(0) &= 0 \\ \theta''(0) &= \frac{1}{sl} \theta'(0) \\ \theta''(l) &= 0 \end{aligned} \right\} \quad (A9)$$

and where

$$\lambda^2 = \frac{2(1 - \mu)a_1 l^2}{a_3 + EI\bar{x}^2 - \frac{(a_2 + EI\bar{x})^2}{a_1 + EI}} \quad (A10)$$

$$GJ = 2(1 - \mu)a_1 \quad (A11)$$

$$Q(y) = M(y) - ecL(y) \quad (A12)$$

$$e = -\frac{a_2 + EI\bar{x}}{c(a_1 + EI)} \quad (A13)$$

$$s = \frac{a_1 + EI}{k_1 l} \quad (A14)$$

The parameter  $GJ$  can be written

$$GJ = G \int_{-c/2}^{c/2} \frac{t^3(x)}{3} dx$$

This quantity then is merely the elementary torsional stiffness for a thin cross section. The quantity  $Q$  is the total moment about an "elastic axis" located  $e$  chords ahead of the midchord. The term "elastic axis" is justified in this case because, as can be seen from equation (A8), loads applied at  $x = -ec$  anywhere along the span would produce no twist. The parameter  $s$  expresses the ratio between the overall stiffnesses of the wing and of the root springs.

In view of the existence of an elastic axis for this configuration, only the influence functions due to torque need be obtained. More specifically, it is desired to calculate the rate of twist  $\frac{d\theta}{dy}$  at station  $y$  caused by the application of a unit torque at station  $\eta$ . This quantity, designated  $\frac{\partial G_m}{\partial y}(y, \eta)$ , can be obtained by solving equation (A8) with the appropriate substitution for  $Q(y)$  and is given by

$$\left. \begin{aligned}
 \frac{\partial G_m}{\partial y}(y, \eta) &= \frac{1}{GJ} \frac{\cosh \lambda \left(1 - \frac{y}{l}\right)}{\cosh \lambda + s\lambda \sinh \lambda} \left( -1 + \cosh \lambda \frac{\eta}{l} + \right. \\
 &\quad \left. s\lambda \sinh \lambda \frac{\eta}{l} \right) \qquad (y > \eta) \\
 \frac{\partial G_m}{\partial y}(y, \eta) &= \frac{1}{GJ} \frac{1}{\cosh \lambda + s\lambda \sinh \lambda} \left\{ \cosh \lambda - \cosh \lambda \left(1 - \frac{y}{l}\right) - \right. \\
 &\quad \left. \sinh \lambda \left(1 - \frac{\eta}{l}\right) \sinh \lambda \frac{y}{l} + \right. \\
 &\quad \left. s\lambda \left[ \sinh \lambda - \sinh \lambda \left(1 - \frac{\eta}{l}\right) \cosh \lambda \frac{y}{l} \right] \right\} \qquad (y < \eta)
 \end{aligned} \right\} \quad (A15)$$

All the quantities in these equations except  $s$  can be found directly from the geometry and material properties of the wing. The parameter  $s$  can be evaluated by equating the theoretical and experimental values of the twist at midspan due to a torque at the tip. Such a process yields the following formula:

$$s = \frac{2 - \operatorname{sech} \frac{\lambda}{2}}{\lambda^2 \left(1 - \frac{2GJ\theta_r}{l}\right)} - \frac{\coth \lambda}{\lambda} \quad (A16)$$

It should be noted that by determining  $s$  in this manner, the torsional characteristics of the wing are duplicated closely. If the value of  $s$  were taken to be zero, the root would be completely clamped and the wing would be too stiff. If, on the other hand, a value of  $s$  equal to infinity were used, the root would be completely free to warp and the wing would be too flexible. For the aluminum wing, for example, taking  $s$  to be zero and infinity would yield, respectively,  $\theta_r$  equal  $0.956 \times 10^{-4}$  and  $1.262 \times 10^{-4}$  radians in.-lb, whereas the actual experimental value is 1.175 radians in.-lb. From these values, it can be seen that appreciable error could result from an improper selection of  $s$ .

In order to evaluate the rate-of-twist influence functions, the quantities  $I$  and  $\bar{x}$  (eqs. (A1) and (A2)) were computed for the nominal

aileron deflection of  $5^\circ$ ; in this calculation, the thickness  $t(x)$  was assumed to vary linearly from its value at the hinge line (see table I) to zero at the trailing edge. The values of  $a_1$ ,  $a_2$ , and  $a_3$  (defined following eq. (A5)) were computed from the airfoil profile data in table I; in this computation, the necessary integrations were performed numerically by using Simpson's rule. The quantities  $\lambda$ , GJ, and  $e$  were then evaluated. (See eqs. (A10), (A11), and (A13).) Finally, equation (A16) was used in conjunction with the experimentally determined values of  $\theta_r$  to find  $s$ . A tabulation of the pertinent parameters for each of the two models follows:

	Steel	Aluminum
$e$ . . . . .	0.0479	0.0485
GJ, lb-in. <sup>2</sup> . . . . .	117,500	42,100
$\lambda$ . . . . .	8.4879	8.3138
$s$ . . . . .	0.0891	0.289

The values of  $\partial G_m / \partial y$  for the aluminum and steel wings have been computed for  $0 < \frac{y}{l} < 1$  in steps of 0.2 and  $0 < \frac{\eta}{l} < 1$  in steps of 0.1. The results are given in table II in matrix form. These matrixes are used directly for the computation of the aeroelastic effects on roll by the method of reference 1.

## REFERENCES

1. Hedgepeth, John M., and Kell, Robert J.: Rolling Effectiveness and Aileron Reversal of Rectangular Wings at Supersonic Speeds. NACA TN 3067, 1954.
2. Strass, H. Kurt, Fields, E. M., and Purser, Paul E.: Experimental Determination of Effect of Structural Rigidity on Rolling Effectiveness of Some Straight and Swept Wings at Mach Numbers From 0.7 to 1.7. NACA RM L50G14b, 1950.
3. Nelson, Robert L.: Large-Scale Flight Measurements of Zero-Lift Drag at Mach Numbers From 0.86 to 1.5 of a Wing-Body Combination Having a 60° Triangular Wing With NACA 65A003 Sections. NACA RM L50D26, 1950.
4. Reissner, Eric, and Stein, Manuel: Torsion and Transverse Bending of Cantilever Plates. NACA TN 2369, 1951.

TABLE I.- DESCRIPTION OF MODELS

## (a) Basic information

Parameter	Steel model	Aluminum model
$l$ , in. . . . .	10.61	10.61
$c$ , in. . . . .	7.07	7.07
$a$ . . . . .	0.236	0.236
$c_a/c$ . . . . .	0.2	0.2
$E$ , psi . . . . .	$29 \times 10^6$	$10.6 \times 10^6$
$\mu$ . . . . .	0.300	0.333
$\theta_r$ , radian/in.-lb . .	$0.392 \times 10^{-4}$	<sup>a</sup> $1.175 \times 10^{-4}$
$\delta$ , deg . . . . .	5.5	4.9

<sup>a</sup>Two values of  $\theta_r$  for the aluminum model were given in reference 2. The value herein is the correct one.

## (b) NACA 65A003 airfoil ordinates

$x/c$	$t/c$	$x/c$	$t/c$	$x/c$	$t/c$	$x/c$	$t/c$
-0.500	0	-0.350	0.02194	0.050	0.02794	0.450	0.00370
-.495	.00464	-.300	.02474	.100	.02606	.500	.00014
-.4925	.00564	-.250	.02688	.150	.02364		
-.4875	.00718	-.200	.02842	.200	.02088		
-.475	.00982	-.150	.02946	.250	.01776		
-.45	.01314	-.100	.02996	.300	.01438		
-.425	.01592	-.050	.02992	.350	.01090		
-.400	.01824	0.0	.02926	.400	.00728		

TABLE II.- RATE-OF-TWIST INFLUENCE-FUNCTION MATRIXES

(a) Steel Wing,  $GJ = 117,500 \text{ lb-in.}^2$ 

$$\left[ \frac{\partial G_M}{\partial y} \right] = \frac{1}{GJ}$$

0	0.246330	0.351742	0.396851	0.416156	0.424417	0.427954	0.429471	0.430127	0.430426	0.430595
0	0.115132	0.398052	0.682758	0.804593	0.856734	0.879056	0.888629	0.892773	0.894659	0.895727
0	0.021085	0.072897	0.195062	0.481008	0.767011	0.889456	0.941967	0.964701	0.975043	0.980904
0	0.003865	0.013364	0.035760	0.088182	0.210716	0.497071	0.783847	0.908006	0.964492	0.996499
0	0.000731	0.002526	0.006760	0.016671	0.039837	0.093973	0.220480	0.516103	0.918371	0.999338
0	0.000259	0.000895	0.002396	0.005908	0.014117	0.033301	0.078132	0.182891	0.427698	0.999765

(b) Aluminum Wing,  $GJ = 42,100 \text{ lb-in.}^2$ 

$$\left[ \frac{\partial G_M}{\partial y} \right] = \frac{1}{GJ}$$

0	0.398616	0.572192	0.647775	0.680688	0.695021	0.701265	0.703991	0.705193	0.705750	0.706073
0	0.144975	0.436856	0.723321	0.848060	0.902382	0.926048	0.936378	0.940933	0.94307	0.944267
0	0.027491	0.082838	0.206553	0.489192	0.771643	0.894695	0.948408	0.972092	0.983085	0.989432
0	0.005219	0.015727	0.039215	0.092874	0.215979	0.498635	0.781750	0.906593	0.964537	0.997994
0	0.001024	0.003085	0.007693	0.018220	0.042370	0.097820	0.225155	0.517578	0.823168	0.999606
0	0.000375	0.001129	0.002816	0.006670	0.015510	0.035909	0.082422	0.189469	0.435303	0.999856

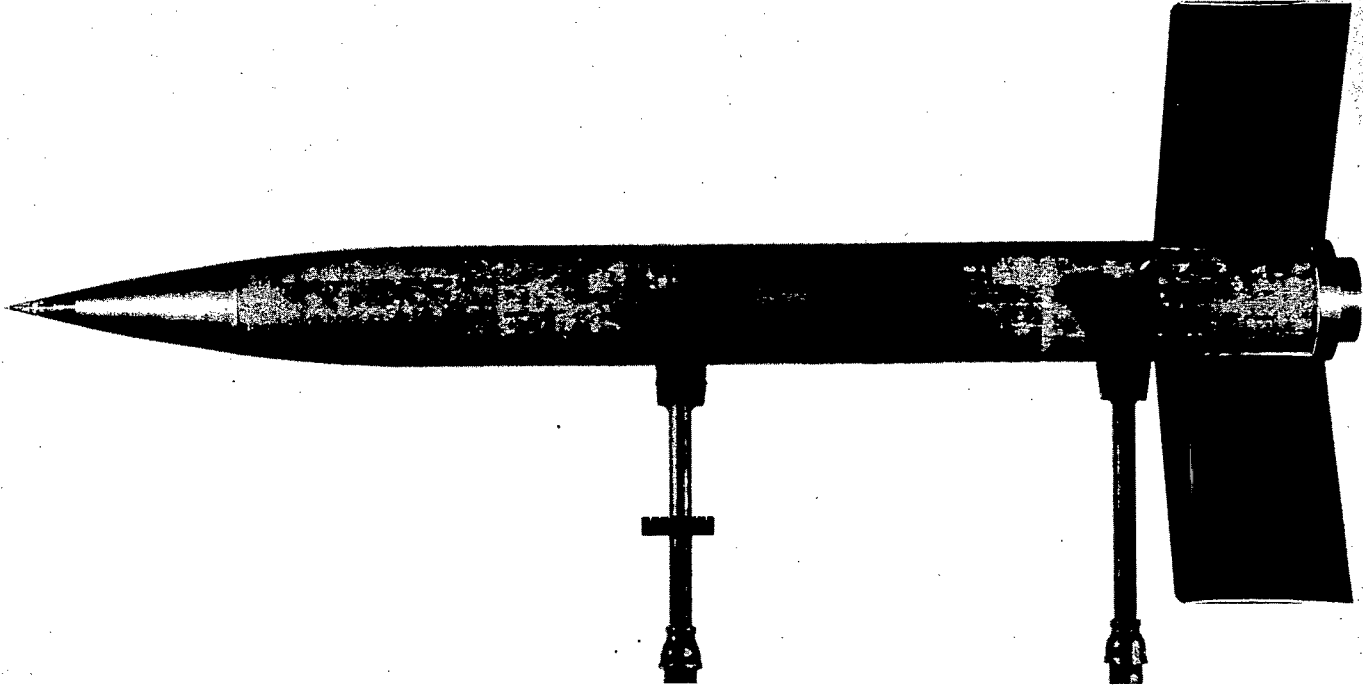


Figure 1.- Test model.

L-71047.1

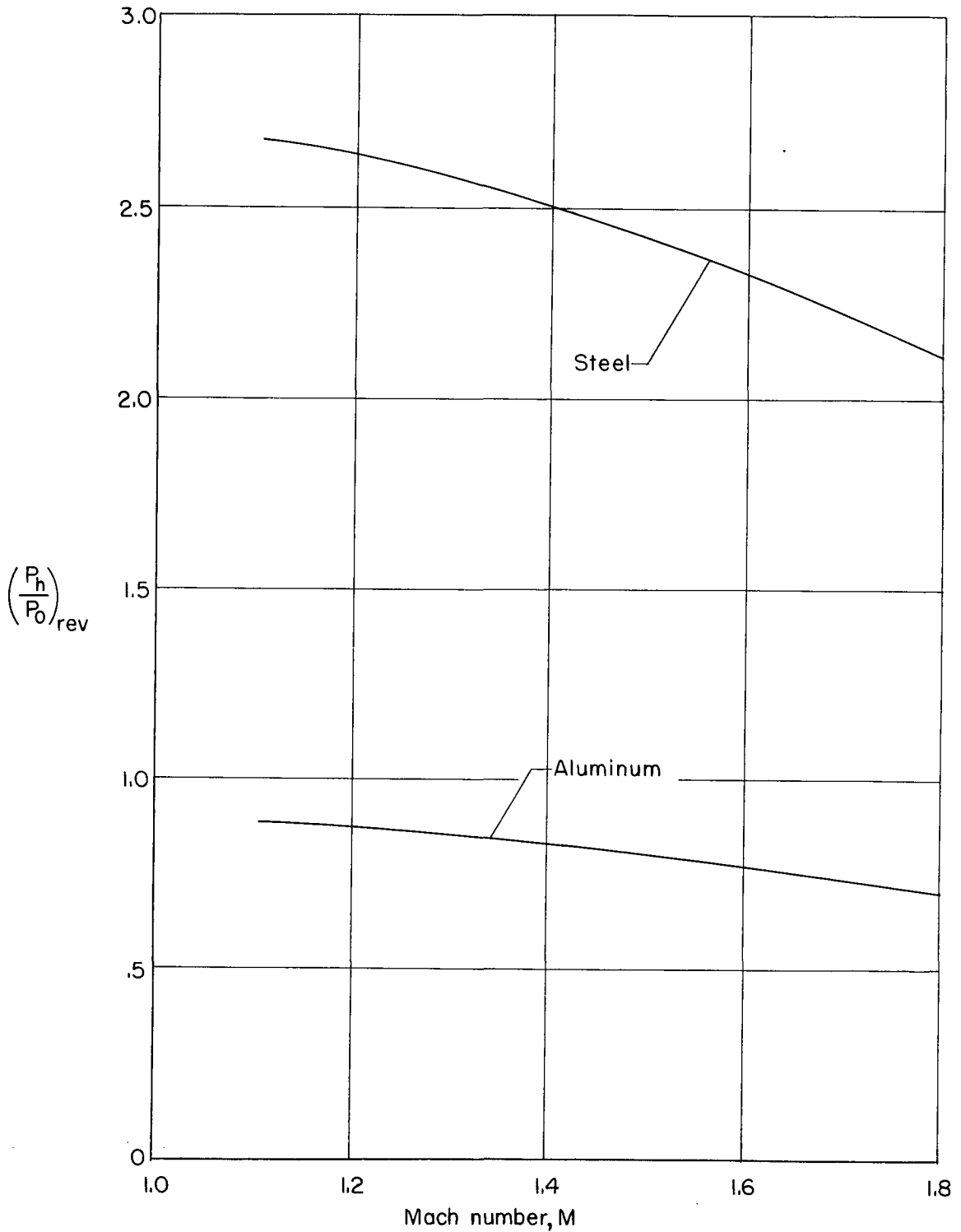


Figure 2.- Variation of pressure ratio at reversal with Mach number for the two models.

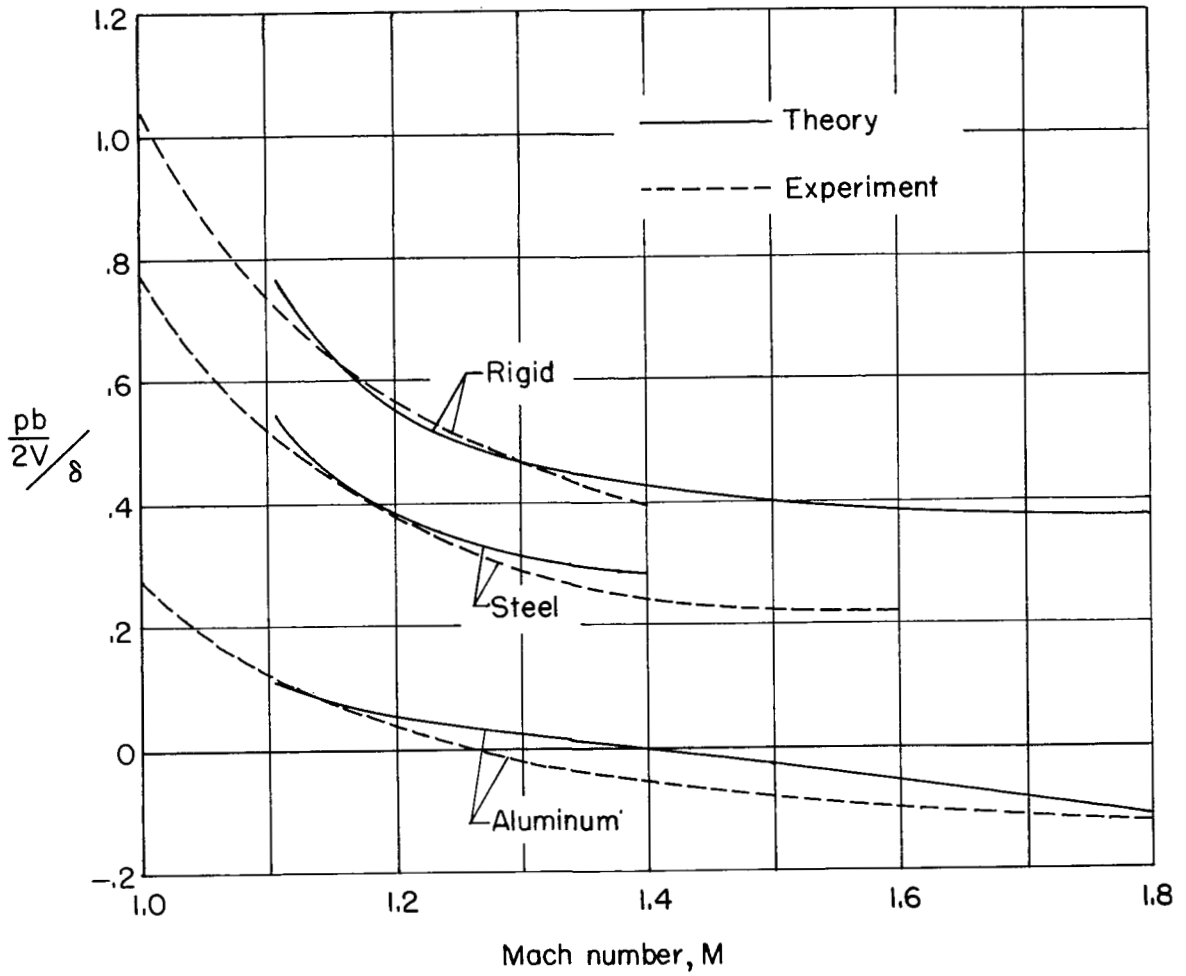
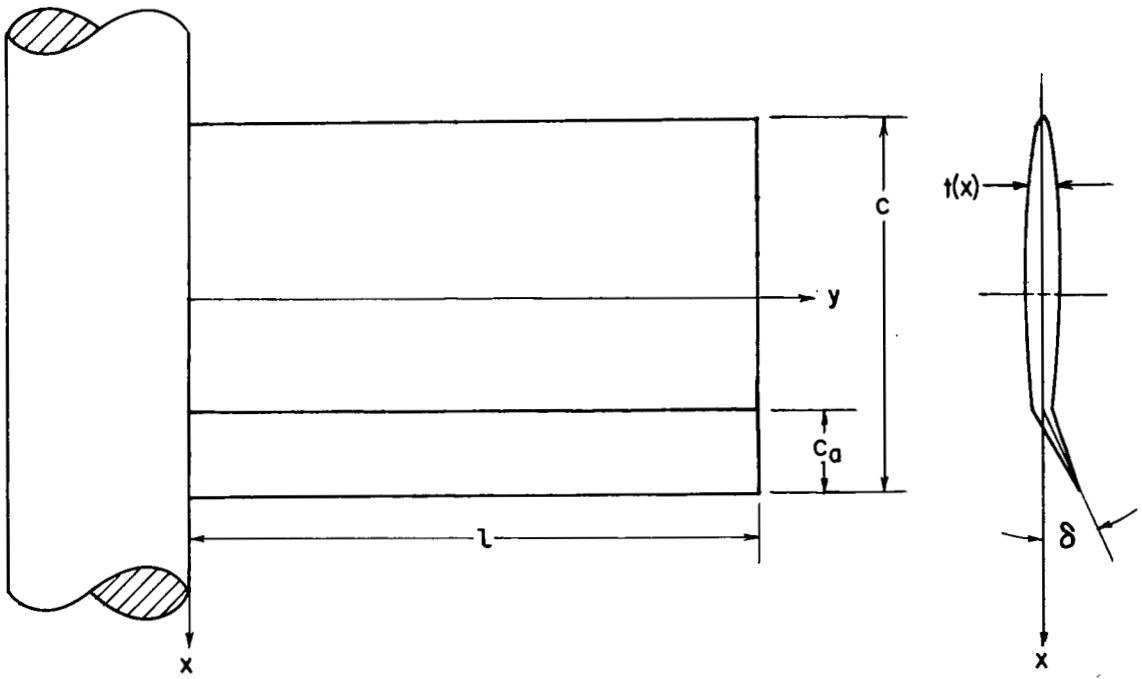
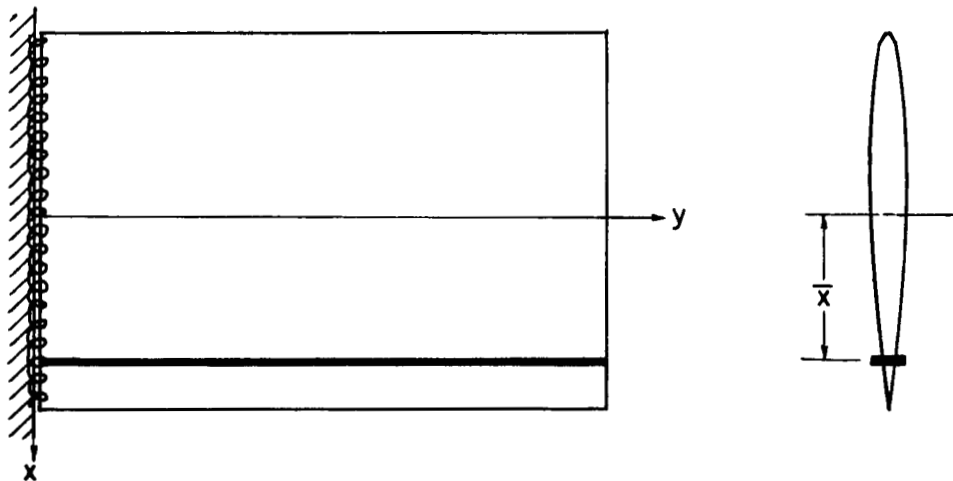


Figure 3.- Variation with Mach number of the theoretical and experimental rate of roll.



(a) Wing with bent-up aileron and flexible root attachment.



(b) Equivalent plate-beam combination mounted on root springs.

Figure 4.- Wing with bent-up aileron and equivalent plate-beam configuration.

~~CONFIDENTIAL~~

NASA Technical Library



3 1176 01437 1612

~~CONFIDENTIAL~~